








# Two New $r$ -process-enhanced Stars with $[\text{Fe}/\text{H}] > -0.6$ dex from the LAMOST-MRS Survey

Xiao-Jin Xie<sup>1,2,3</sup> , Jian-Rong Shi<sup>2,4</sup> , Tian-Lu Chen<sup>1,3</sup> , Hong-Liang Yan<sup>2,4</sup>, Tian-Yi Chen<sup>2,4</sup> , Kai-Ke Pan<sup>5,6</sup>,  
Chun-Qian Li<sup>2,4</sup>, Shuai Liu<sup>2,4</sup> , Qi Gao<sup>2,4</sup>, Tai-Sheng Yan<sup>2,4</sup>, and Ming-Yi Ding<sup>2,4</sup>

<sup>1</sup>Department of Physics, College of Science, Tibet University, Lhasa 850000, China

<sup>2</sup>Key Laboratory of Optical Astronomy, National Astronomical Observatories, Chinese Academy of Sciences, Beijing 100101, China; [sjr@bao.ac.cn](mailto:sjr@bao.ac.cn)

<sup>3</sup>Key Laboratory of Cosmic Rays (Tibet University), Ministry of Education, Lhasa 850000, China; [chentl@utibet.edu.cn](mailto:chentl@utibet.edu.cn)

<sup>4</sup>School of Astronomy and Space Science, University of Chinese Academy of Sciences, Beijing 100049, China

<sup>5</sup>Apache Point Observatory, Sunspot, New Mexico 88349, USA

<sup>6</sup>Astronomy Department, New Mexico State University, Las Cruces, New Mexico 88003, USA

Received 2022 February 25; revised 2022 May 2; accepted 2022 May 5; published 2022 June 14

## Abstract

We report the discovery of two  $r$ -process-enhanced stars with  $[\text{Fe}/\text{H}] > -0.6$  dex selected from the Large Sky Area Multi-Object Fiber Spectroscopic Telescope (LAMOST) survey. Three candidate stars have been selected from the LAMOST medium-resolution ( $R \sim 7500$ ) spectroscopic survey, and the followed-up high signal-to-noise ratio and high-resolution ( $R \sim 31,500$ ) spectra are obtained with the ARC Echelle Spectrograph mounted on the 3.5 m telescope at the Apache Point Observatory, which allow us for the determination of stellar atmospheric parameters and abundances of 20 elements. Among these three  $r$ -process-enhanced candidate stars, TYC 1710-933-1 and TYC 2858-372-1 have  $[\text{Eu}/\text{Fe}]$  higher than 0.3 dex and  $[\text{Ba}/\text{Eu}]$  lower than 0.0 dex, thus, can be identified as new  $r$ -process-enhanced objects. TYC 2858-372-1 shows similar  $r+s$ -process pattern to the Sun. TYC 1710-933-1 presents enhancement of the  $r$ -process elements of Nd and Eu. Our work indicates that the enrichment mechanisms of the heavy neutron-capture elements are complicated for metal-rich stars.

*Key words:* stars: abundances – stars: chemically peculiar – stars: fundamental parameters

## 1. Introduction

It is known that about half elements heavier than iron are produced by the rapid neutron-capture process ( $r$ -process, Burbidge et al. 1957; Cameron 1957), and several astrophysical sites have been suggested, such as neutron star mergers (NSMs, Lattimer & Schramm 1974; Rosswog et al. 2014; Thielemann et al. 2017), core-collapse supernovae (e.g., Sato 1974; Witt et al. 1994; Farouqi et al. 2010; Mirizzi 2015; Tsujimoto 2021), magneto-rotational jet-driven supernovae (e.g., Symbalisty et al. 1985; Fujimoto et al. 2008; Nishimura et al. 2015; Obergaulinger et al. 2018), collapsars (Siegel et al. 2019), and common envelope jets supernova (Papish et al. 2015; Grichener & Soker 2019). Although, the NSM was identified as an indeed site of  $r$ -process nucleosynthesis (Pian et al. 2017; Kasen et al. 2017; Watson et al. 2019), recent studies showed that multiple sites are needed to explain the  $r$ -process abundance patterns (e.g., Côté et al. 2018; Hotokezaka et al. 2018; Côté et al. 2019; Siegel 2019; Brauer et al. 2021; Farouqi et al. 2021; Tsujimoto 2021; Yamazaki et al. 2021; Naidu et al. 2022).

Observations of the abundance patterns of  $r$ -process elements for a large amount of sample stars will be very helpful to constrain the fundamental physics and site(s) behind the  $r$ -process (Beers & Christlieb 2005). Based on the large spectra surveys, such as the Hamburg/ESO Survey (HES,

Christlieb et al. 2004; Barklem et al. 2005) and the  $R$ -Process Alliance (RPA) survey (Hansen et al. 2018; Gudin et al. 2021), over four hundreds  $r$ -process-enhanced metal-poor stars have been found (Hansen et al. 2018; Abohalima & Frebel 2018; Sakari et al. 2018; Ezzeddine et al. 2020; Holmbeck et al. 2020). It is found that their abundance patterns have good consistence for Ba to Hf in all types of stars, while have variations among the lightest and heaviest elements (e.g., Sneden et al. 1994; Roederer et al. 2014; Aoki et al. 2017; Sakari et al. 2018). More recently, Cowan et al. (2021) noted that all the extreme  $r$ -process-rich stars ( $r$ -II,  $[\text{Eu}/\text{Fe}] > +1.0$  dex) show similar abundance patterns in the heavy neutron-capture elements, however, the  $r$ -I stars present abrupt dropoffs in abundance through the rare-earth domain.

The previous works are concentrated on metal-poor stars of  $[\text{Fe}/\text{H}] > -1.0$  dex, while no systematic study, to our knowledge, has focused on the  $r$ -process elements enhanced stars with  $[\text{Fe}/\text{H}]$  over  $-1.0$  dex. In this paper, we report the high-resolution spectroscopic study to three  $r$ -process-enhanced (RPE) candidates found by the Large Sky Area Multi-Object Fiber Spectroscopic Telescope (LAMOST) medium-resolution spectroscopic survey (Chen et al. 2021). This paper is outlined as follows. The observations and data reduction are described in Section 2. The determination of stellar atmospheric parameters is

**Table 1**  
Observations Log

Name	R.A. (J2000)	Decl.	V mag	MJD	Exp Time (s)	RV <sub>helio</sub> (km s <sup>-1</sup> )	Parallax (mas)	Other Identifier
TYC1710-933-1	22:51:46.00	22:28:19.20	11.881	58 769	1450	-34.2	0.6166 <sup>a</sup>	2MASSJ22514592+2228190
TYC2858-372-1	2:52:40.90	44:18:02.30	11.387	58 796	1680	-1.7	0.5534 <sup>a</sup>	2MASSJ02524087+4418024
TYC3143-542-1	19:30:54.50	41:52:37.40	11.442	58 769	1500	-14.2	1.9059 <sup>a</sup>	2MASSJ19305460+4152375

**Note.**<sup>a</sup> Gaia Collaboration (2018).**Table 2**  
The Stellar Parameters of the Program Stars

Name	$T_{\text{eff}}$ (K)	log $g$	[Fe/H]	$\xi$ (km s <sup>-1</sup> )	$U$ (km s <sup>-1</sup> )	$V$ (km s <sup>-1</sup> )	$W$ (km s <sup>-1</sup> )
TYC1710-933-1	5075	2.77	-0.38	1.7	55.39	-34.78	9.46
TYC2858-372-1	4195	1.74	-0.27	1.2	-32.11	-38.37	24.45
TYC3143-542-1	6227	3.87	-0.56	2.2	9.37	-19.71	10.29

presented in Section 3, and the analyses of chemical abundances are shown in Section 4. The discussion of our results and the summary are provided in Sections 5 and 6, respectively.

## 2. Observation and Data Reduction

The three RPE candidates have been selected from the LAMOST (Cui et al. 2012; Yan et al. 2022) medium-resolution ( $R \sim 7500$ ) spectroscopic survey by matching the observed spectra to the synthetic templates around the Eu II line at 6645.1 Å (Chen et al. 2021). We only select the objects with [Eu/Fe] > 0.3 dex and Vmag < 12. The follow-up high signal-to-noise ratio (S/N) and high-resolution spectra of three program stars are obtained with the Astrophysical Research Consortium (ARC) Echelle Spectrograph mounted on the 3.5 m telescope at the Apache Point Observatory. The observed spectra cover the wavelength range of 4000–9000 Å with a resolving power of  $R \sim 31,500$ , and the S/N of the spectra is round 60 at 5600 Å. We present the observation information in Table 1.

The raw 2D spectra have been reduced by using the Interactive Data Language (IDL) programs for background subtraction, flat-fielding, order identification, extraction and wavelength calibration (Pfeiffer et al. 1998).

## 3. Stellar Atmospheric Parameters

Based on the MARCS stellar atmospheric models (Gustafsson et al. 2008), we derive the stellar atmospheric parameters, i.e., the effective temperature ( $T_{\text{eff}}$ ), surface gravity (log  $g$ ), metallicity ([Fe/H]), and microturbulent velocity ( $\xi$ ) for our three program stars by the spectroscopic approach method. The effective temperatures are derived from the excitation

equilibrium of Fe I lines with an excitation energy ( $E_{\text{exc}}$ ) higher than 2.0 eV (Sitnova et al. 2015). The surface gravities are determined by the ionization equilibrium of Fe I and Fe II lines, and the microturbulent velocities are derived by forcing the iron abundances from different Fe I lines independent of their equivalent widths (EW). The metallicity can be settled simultaneously if all the aforementioned constraints are achieved. In our analysis, the line data of Fe I and Fe II lines are taken from Yan et al. (2018). The abundance analysis is based on 1D local thermal equilibrium (LTE) unless otherwise stated. Sitnova et al. (2015) found that the non-local thermal equilibrium (NLTE) effects of iron are less than 0.06 dex for this type of stars.

The final stellar atmospheric parameters of our three target stars are presented in Table 2. We show the derived iron abundances of individual Fe I and Fe II lines as functions of their excitation potentials (top panel) and equivalent widths (bottom panel) for TYC 1710-933-1 in Figure 1. The uncertainties on the effective temperature, surface gravity, iron abundance and microturbulent velocity by this method are about 100 K, 0.2 dex, 0.1 dex and 0.2 km s<sup>-1</sup>, respectively.

## 4. Abundance Analysis

### 4.1. Atomic Data

The abundances of 20 elements, namely C, N, O, Na, Mg, Al, Si, Ca, Sc, Ti, Ni, Cu, Sr, Y, Zr, Ba, La, Ce, Nd and Eu are derived for program stars, and the atomic data for C I, N I, O I, Na I, Mg I, Al I, Si I, Ca I, Sc II, Ti II, Cu I, Zr II, Sr II, Ba II and Eu II lines are adopted from Zhao et al. (2016). The atomic data for Ni I, Sr I, Y II, La II, Ce II and Nd II lines are selected from Roederer et al. (2018), and we have slightly revised the log  $gf$  values by fitting the solar spectrum with the LTE assumption. It

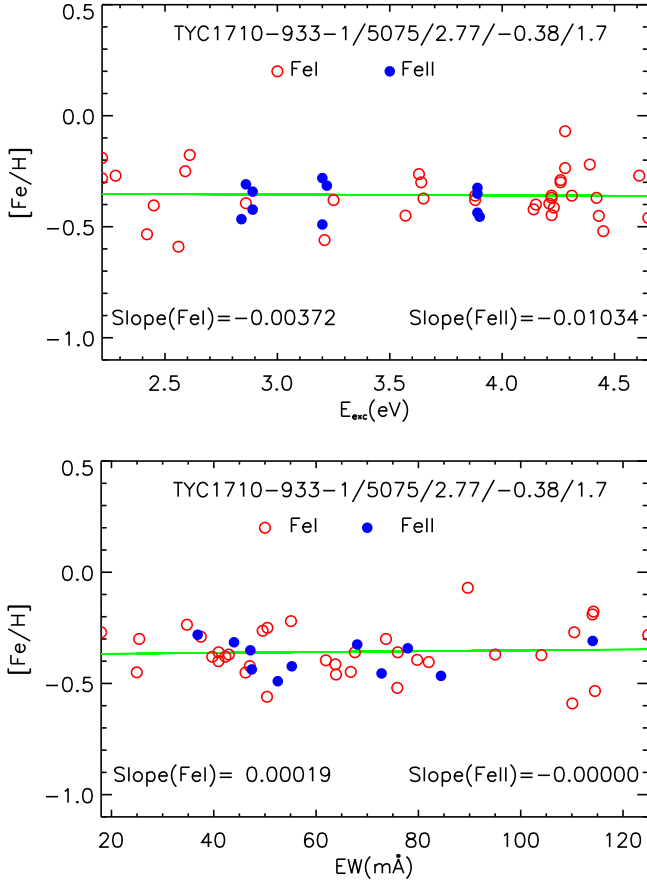


**Figure 1.** The determination of stellar atmospheric parameters of TYC 1710-933-1 based on the ionization and excitation equilibrium of Fe I and Fe II lines. The open red circles refer to Fe I lines. The filled blue circles are for Fe II lines. The green straight lines are the fitting results with the least square method.

is noted that the hyperfine structure (HFS) of strong absorption lines cannot be ignored when deriving the abundances of Sc, Cu, Sr, Ba and Eu, and therefore, HFS of lines for these elements has been considered. The adopted atomic parameters and their references are listed in Table 3.

#### 4.2. Abundance Determination

The abundances of all 20 elements are derived with the spectrum synthesis method. The theoretical line profiles are calculated by an interactive IDL code Spectrum Investigation Utility (SIU, Reetz 1991) using the MARCS stellar model atmospheres (Gustafsson et al. 2008). The solar abundances are adopted from Asplund et al. (2009).

The C abundance of TYC 3143-542-1 is derived from four C I lines, but only 5380 Å line for TYC 710-933-1 and only 8335 Å line for TYC 2858-372-1 are used, as the other lines are too weak for these two stars.

The N abundance can be obtained from both the N I line at 7468 Å and CN bands, but the 7468 Å line of TYC 1710-933-1

is too weak to obtain reliable abundance. Therefore, we fix the C abundance to determine the N abundance from the CN bands around 8003 Å, and the line data around CN bands are adopted from Carlberg et al. (2012).

For O, the abundances of TYC 1710-933-1 and TYC 2858-372-1 are obtained by fitting the forbidden [O I] line at 6300 Å. The [O I] line of TYC 3143-542-1 is blended with an emission feature. Thus, we use the O I triplet lines at 7771–7775 Å to derive its O abundance. The NLTE effects from Sitnova et al. (2013) have been considered for O I line.

The elements of Ba and Eu are very important for classification of the RPE stars. It is found that the NLTE effects cannot be ignored for both Ba and Eu (Zhao et al. 2016). Hence, the Ba and Eu abundances are derived with NLTE effects taken into consideration. The atomic models of Ba and Eu are adopted from Mashonkina et al. (1999) and Mashonkina & Gehren (2001), respectively.

The final abundances are given in Table 4. The uncertainties shown for each element in Table 4 are the statistical standard deviation of different spectral lines.

#### 4.3. Abundances Uncertainties

The uncertainties of stellar atmospheric parameters lead to errors in the abundance results. We change each stellar parameter with its typical uncertainty to investigate the impact on the derived elemental abundances. In Table 5, we show the result for TYC 1710-933-1 as an example. The total errors (the last column in Table 5) are square roots of the quadratic sum of errors associated with the four stellar parameters. As shown in Table 5, the uncertainties of all the elements due to errors of the stellar parameters are less than 0.15 dex.

## 5. Discussion

### 5.1. Light Elements ( $Z < 30$ )

The abundance distribution of 20 elements along with their error bars for the three objects are shown in Figure 2. Two evolved stars, i.e., TYC 1710-933-1 and TYC 2858-372-1, show deficient C and over-abundance of N and O, which is a result of stellar evolution. The balanced CNO cycle ultimately alters the ratio of the nuclei, making  $^{14}\text{N}$  the most abundant one. These newly synthesized materials are circulated from the interior to the surface by the enhanced convection of the evolved stars. The highly evolved states of these two stars can also be inferred from the low surface gravities. As a contrast, TYC 3143-542-1 shows a much higher ratio of [C/N] and a solar value for O, coinciding with its low evolved state.

The kinematic information shows that TYC 1710-933-1 is a thin-disk star (Table 2), whereas its Mg abundance is notably different from either field stars (e.g., Sneden et al. 2008) or stars in globular clusters (GC, Pancino et al. 2017) of its metallicity. Similar discrepancy can also be clearly seen from

**Table 3**  
The Lines used for Abundance Analyses

Ion	$\lambda$ (Å)	$\chi$ (eV)	$\log gf$	Ion	$\lambda$ (Å)	$\chi$ (eV)	$\log gf$
C I	4932.05	7.68	-1.66	Sc II	5669.03 <sup>a</sup>	1.49	-1.20
C I	5052.14	7.68	-1.30	Sc II	6245.63 <sup>a</sup>	1.50	-1.03
C I	5380.33	7.68	-1.62	Ti II	5005.16	1.57	-2.73
C I	8335.15	7.68	-0.44	Ti II	5185.90	1.89	-1.41
N I	7468.31	10.34	-0.11	Ti II	5211.53	2.59	-1.41
O I	7771.94	9.15	0.37	Ti II	5336.79	1.58	-1.60
[O I]	6300.30	0.00	-9.78	Ti II	5381.02	1.57	-1.97
Na I	5682.64	2.10	-0.71	Ti II	5418.77	1.58	-2.13
Na I	5688.21	2.10	-0.41	Ni I	6643.63	1.68	-2.22
Na I	6154.23	2.10	-1.55	Ni I	6767.77	1.82	-2.14
Mg I	4571.09	0.00	-5.47	Cu I	5105.54 <sup>a</sup>	1.39	-1.52
Mg I	4702.99	4.34	-0.38	Cu I	5218.20 <sup>a</sup>	3.82	0.48
Mg I	5528.41	4.34	-0.47	Cu I	5782.13 <sup>a</sup>	1.64	-1.72
Mg I	5711.07	4.34	-1.64	Sr I	4607.33 <sup>b</sup>	0.00	0.09
Al I	6696.03	3.14	-1.51	Sr II	4077.71 <sup>a</sup>	0.00	0.15
Al I	6698.67	3.14	-1.87	Sr II	4215.52 <sup>a</sup>	0.00	-0.17
Al I	7835.31	4.02	-0.65	Y II	4854.86	0.99	-0.27
Al I	7836.13	4.02	-0.49	Y II	4883.68	1.08	0.19
Si I	5690.42	4.71	-1.74	Zr II	4317.31	0.71	-1.45
Si I	5701.10	4.71	-1.96	Zr II	5112.27	1.66	-0.85
Si I	5772.15	5.08	-1.62	Ba II	4554.03 <sup>a</sup>	0.00	0.17
Si I	6142.48	5.62	-1.48	Ba II	5853.67	0.60	-1.00
Si I	6145.02	5.62	-1.39	Ba II	6141.71	0.70	-0.08
Si I	6155.13	5.62	-0.78	Ba II	6496.90	0.60	-0.38
Ca I	5512.98	2.93	-0.46	La II	4123.22	0.32	0.13
Ca I	5588.75	2.53	0.36	La II	4333.75	0.17	-0.06
Ca I	5590.12	2.51	-0.57	La II	5303.53	0.32	-1.35
Ca I	5857.45	2.93	0.24	La II	6390.48	0.32	-1.41
Ca I	5867.57	2.93	-1.57	Ce II	4120.83	0.32	-0.37
Ca I	6161.29	2.51	-1.27	Ce II	4418.78	0.86	0.42
Ca I	6162.17	1.90	-0.09	Ce II	4562.36	0.48	0.21
Ca I	6166.44	2.51	-1.14	Ce II	4628.16	0.52	0.08
Ca I	6169.06	2.51	-0.80	Nd II	4446.38	0.20	-0.51
Ca I	6169.56	2.53	-0.48	Nd II	4959.12	0.06	-0.80
Sc II	5031.02 <sup>a</sup>	1.35	-0.40	Nd II	5319.81	0.55	-0.28
Sc II	5526.81 <sup>a</sup>	1.76	-2.11	Eu II	4129.72 <sup>a</sup>	0.00	0.22
Sc II	5640.97 <sup>a</sup>	1.49	-1.13	Eu II	4205.02 <sup>a</sup>	0.00	0.21
Sc II	5657.87 <sup>a</sup>	1.50	-0.60	Eu II	6645.06 <sup>b</sup>	1.38	0.12
Sc II	5667.16 <sup>a</sup>	1.49	-1.31				

**Notes.**<sup>a</sup> HFS, Zhao et al. (2016).<sup>b</sup> HFS, Roederer et al. (2018).

the Si abundance. The deficient Mg and Si abundances indicate that TYC 1710-933-1 might be a star from accreted dwarf galaxies (e.g., Xing et al. 2019), where the chemical evolution is slower than that of our Milky Way. Furthermore, the Na and Al abundances of this star indicate that it may belong to the dwarf galaxy populations if following the definition suggested by Fernández-Trincado et al. (2021). In such a case, the stars in dwarf galaxies generally have a slower chemical evolution history compared to the MW stars, allowing long timescale event to take place more frequently, such as the NSM which have been considered as one of the promising enrichment

sources of *r*-process elements. However, it is worth doubting that whether dwarf galaxy with such high metallicity is a common case, as most of the dwarf galaxies reported so far are with metallicity below  $-1.0$  dex. If TYC 1710-933-1 is not from dwarf galaxy, there could be unrevealed mechanism that leads to this strange pattern, which merits further investigation.

As a contrast, TYC 2858-372-1, another thin-disk star with second high abundance of *r*-process elements in our sample, shows a typical Mg abundance (or alpha-abundance) compared to the field stars. Similar to many metal-poor RPE stars found in stellar streams of our Milky Way, this star also shows no

**Table 4**  
The Derived Abundances of 20 Elements for the three Program Stars

Species	TYC 1710-933-1 [X/Fe] (dex)	Number of lines	TYC 2858-372-1 [X/Fe] (dex)	Number of lines	TYC 3143-542-1 [X/Fe] (dex)	Number of lines
C I	0.24	1	0.03	1	0.17 ± 0.02	4
N I	<0.69	1	0.42	1	0.02	1
N(CN)	0.41 ± 0.02	2	0.45 ± 0.05	2	...	—
[O I]	0.14	1	0.36	1	...	...
O I (LTE)	...	...	...	...	0.31	3
O I (NLTE)	...	...	...	...	−0.03	3
Na I	0.26 ± 0.04	3	0.12 ± 0.03	3	0.28 ± 0.03	3
Mg I	−0.30 ± 0.05	3	0.07 ± 0.02	3	−0.09 ± 0.06	4
Al I	0.27 ± 0.02	4	0.26 ± 0.02	3	0.26 ± 0.04	3
Si I	−0.30 ± 0.04	4	0.02 ± 0.03	5	0.01 ± 0.05	6
Ca I	0.06 ± 0.04	8	0.16 ± 0.07	10	0.15 ± 0.03	9
Sc II	0.07 ± 0.06	6	0.00 ± 0.06	5	0.13 ± 0.04	7
Ti II	0.14 ± 0.05	6	0.23 ± 0.09	5	0.13 ± 0.03	5
Ni I	0.28 ± 0.04	2	0.14 ± 0.01	2	0.06 ± 0.01	2
Cu I	−0.06 ± 0.03	3	0.02 ± 0.14	3	−0.01 ± 0.05	3
Sr I	0.03	1	−0.14	1	0.10	1
Sr II	...	...	−0.19 ± 0.01	2	0.03 ± 0.03	2
Y II	−0.18 ± 0.03	2	−0.21 ± 0.02	2	−0.07 ± 0.01	2
Zr II	0.21 ± 0.02	2	0.39 ± 0.01	2	0.03 ± 0.03	2
Ba II (LTE)	0.14 ± 0.06	3	0.28 ± 0.07	4	0.12 ± 0.13	3
Ba II (NLTE)	−0.02 ± 0.05	3	0.23 ± 0.06	4	−0.07 ± 0.15	3
La II	0.11 ± 0.01	4	0.20 ± 0.01	2	0.15 ± 0.02	3
Ce II	0.01 ± 0.04	4	−0.05 ± 0.06	3	0.20 ± 0.02	3
Nd II	0.52 ± 0.11	3	0.32 ± 0.07	3	0.16	1
Eu II (LTE)	0.60	1	0.36 ± 0.01	3	0.22	1
Eu II(NLTE)	0.57	1	0.40 ± 0.06	3	0.29	1

**Table 5**  
The Uncertainties of Elemental Abundances due to the Errors of Stellar Atmospheric Parameters for TYC 1710-933-1

$\Delta$ [X/Fe]	$\Delta T_{\text{eff}}$ +100 K	$\Delta \log g$ +0.2 dex	$\Delta$ [Fe/H] +0.1 dex	$\Delta \xi$ +0.2 km s <sup>−1</sup>	$\Delta$ Total dex
C I	0.04	0.08	−0.03	0.03	0.10
N(CN)	0.02	0.03	−0.02	−0.06	0.07
[O I]	−0.10	0.04	−0.08	−0.01	0.13
Na I	0.06	−0.02	−0.04	0.00	0.07
Mg I	−0.01	−0.04	−0.06	0.00	0.07
Al I	0.05	0.02	−0.06	0.00	0.08
Si I	0.05	0.00	0.01	−0.02	0.05
Ca I	0.02	−0.01	−0.10	−0.02	0.10
Sc II	0.03	0.01	−0.08	0.00	0.09
Ti II	0.07	0.00	−0.06	−0.02	0.09
Ni I	0.00	0.03	−0.05	−0.03	0.07
Cu I	−0.01	0.02	−0.05	−0.02	0.06
Sr I	0.06	0.01	−0.04	−0.04	0.08
Y II	0.06	0.04	−0.06	−0.03	0.10
Zr II	0.07	−0.01	−0.03	−0.06	0.10
Ba II	0.00	0.03	−0.03	−0.05	0.07
La II	0.01	0.04	−0.07	−0.02	0.08
Ce II	0.01	0.04	−0.03	−0.05	0.07
Nd II	0.05	0.04	−0.01	−0.03	0.07
Eu II	0.02	0.04	−0.04	−0.04	0.07

sign of enhanced Na or Al abundances (Gull et al. 2021). Its abundances of elements with  $Z < 30$  generally agree with the disk field stars (Fernández-Trincado et al. 2021). This indicates that TYC 2858-372-1 is a local resident of our Milky Way, which is far different from TYC 1710-933-1. Unfortunately, there is insufficient information at this stage to infer the enhancement mechanism of  $r$ -process elements in such metal-rich field stars.

TYC 3143-542-1 is the most metal-poor star in our sample. Its Mg and Si abundances are also slightly lower, but still within the lower boundary of field stars (e.g., Sneden et al. 2008). Considering its relatively high Na and Al abundances, this star could be either from GC, GC debris or dwarf galaxy. Since it has not highly evolved, its low N abundance can be used as an indicator to rule out GC debris (see Figure 1 of Fernández-Trincado et al. 2021).

The distinct alpha-abundance patterns, possibly different birthplaces, and the relatively high metallicities among our RPE stars indicate that the enrichment mechanisms of the heavy neutron-capture elements for the metal-rich stars are complicated.

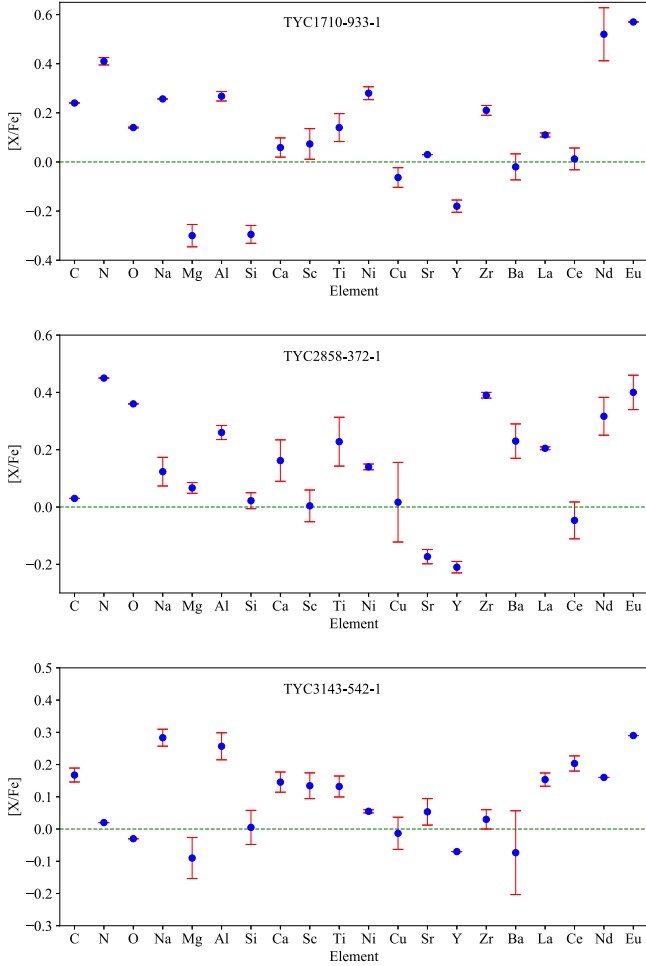


**Figure 2.** The elemental abundances with error bars for our three program stars.

### 5.2. Heavy Elements

It can be seen from Figure 2 that both TYC 1710-933-1 and TYC 2858-372-1 present enhancements of Nd and Eu. The  $[\text{Eu}/\text{Fe}]$  ratios of TYC 1710-933-1 and TYC 2858-372-1 are +0.57 dex and +0.40 dex, and the  $[\text{Ba}/\text{Eu}]$  ratios are  $-0.59$  dex and  $-0.17$  dex, respectively. These two stars are moderately enhanced in Eu, a typical  $r$ -process element, which confirms that TYC 1710-933-1 and TYC 2858-372-1 are two RPE stars. As to TYC3143-542-1, its ratios of  $[\text{Eu}/\text{Fe}]$ ,  $[\text{Sr}/\text{Ba}]$ , and  $[\text{Sr}/\text{Eu}]$  are +0.29 dex, 0.12 dex, and  $-0.24$  dex, respectively. The Eu is only slightly enhanced compared to the other two stars.

The three program stars have high metallicities, which indicates that they may have experienced both  $r$ - and  $s$ -process

events more than metal-poor counterparts. It is fair to compare the abundance patterns of the program stars with those with similar metallicities. From the viewpoint of the availability of the data, it is reasonable to compare them with the solar abundances. In Figures 3, 4, and 5, we plot abundances of the neutron capture elements for the three objects along with the solar  $s$ -,  $r$ - and  $r+s$ -process values.

As shown in Figure 3, for TYC 1710-933-1, the abundances of  $s$ -process dominant elements, such as Sr, Y, Zr, Ba, La and Ce, are consistent with the solar  $s$ -process pattern, while the elements of Nd and Eu, which are mainly produced by the  $r$ -process, are obviously higher than those of the solar  $s$ -process abundance. Compared to the solar  $r+s$ -process abundances, we can still see that Nd and Eu are over-abundant, which supports the result that this star is enhanced with  $r$ -process elements.

As for TYC 2858-372-1, its  $s$ -process elements including Zr, Ba and La are consistent with the solar  $s$ -process abundance pattern, while Ce is slightly lower than that of the solar  $s$ -process value. Compared to the solar  $r+s$ -process abundance pattern, the heavy neutron capture elements, such as Ba, La, Nd and Eu can be well represented, although Ce shows slightly lower value, which means that they may have similar origin to the Sun. However, the light neutron-capture elements, such as Sr and Y, present much lower values.

The abundances of heavy neutron capture elements of TYC 3143-542-1 are enhanced when compared to the solar  $r+s$  one as shown in Figure 5. The light neutron capture elements, including Sr, Y and Zr, are consistent with the solar  $r+s$  ones, and the abundances of La, Ce, Nd, Eu are enhanced relative to the solar  $r+s$  values. This result indicates that this object may also have enhanced  $r$ -process elements.

## 6. Summary

We study the neutron-capture elements of three stars at high metallicities ( $[\text{Fe}/\text{H}] > -0.6$  dex) with possible enhancements of heavy  $r$ -process elements, and report the discovery of two  $r$ -process-enhanced stars among them. TYC 1710-933-1 has a  $[\text{Eu}/\text{Fe}]$  of 0.57 dex, and TYC 2858-372-1 has a  $[\text{Eu}/\text{Fe}]$  of 0.40 dex. Both of the RPE stars exhibit low ratios of  $[\text{Ba}/\text{Eu}]$  ( $< 0.0$  dex). The two RPE stars also show enhancement of Nd as seen from the abundance patterns, while TYC 2858-372-1 shows similar abundance pattern to the Sun. The RPE stars found in this work are more metal-rich than previous RPE stars whose metallicities are usually below  $-1.0$  dex. This means that the enrichment mechanisms of the heavy neutron-capture elements are complicated, and hence we need more examples of this type star for investigation. The results reported in this paper are part of the program of searching for the RPE stars from the LAMOST survey.

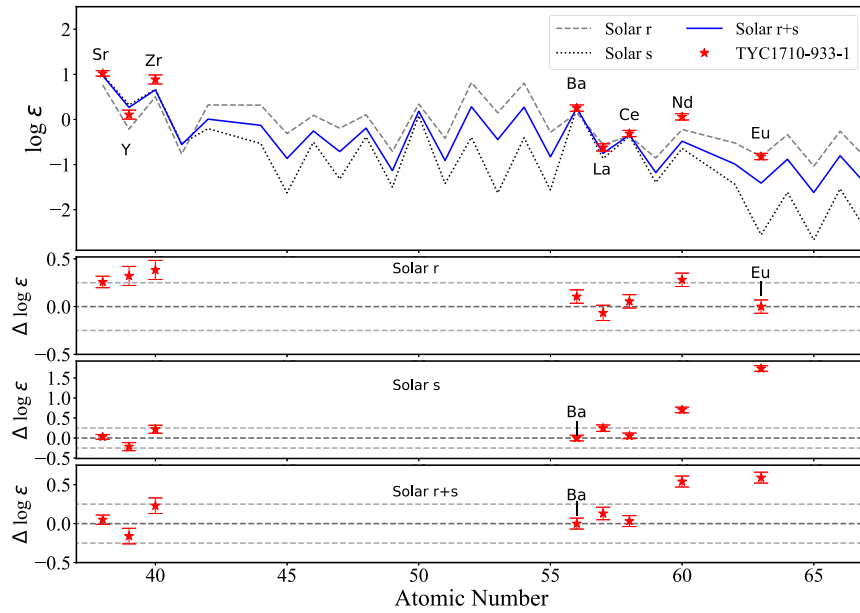


**Figure 3.** Top panel: the abundances of neutron-capture elements of TYC 1710-933-1 with the error bars. Also shown are the  $r$ -,  $s$ - and  $r+s$  patterns of the solar system. The solar  $r$ -process pattern is shifted to the Eu abundance, while the solar  $s$ - and  $r+s$  patterns are shifted to match the Ba abundance. The three bottom panels: abundance offsets between TYC 1710-933-1 and the solar system.

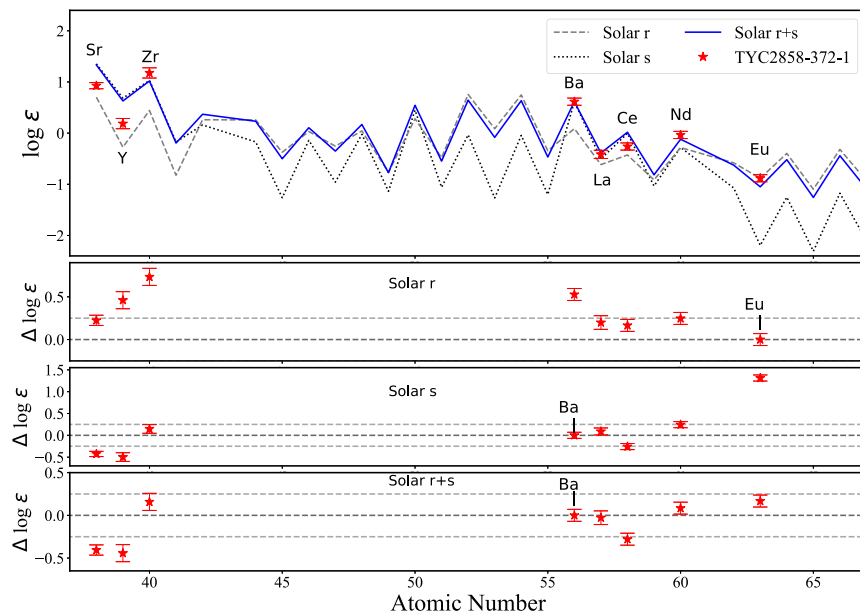


**Figure 4.** Similar to Figure 3, but for TYC 2858-372-1.

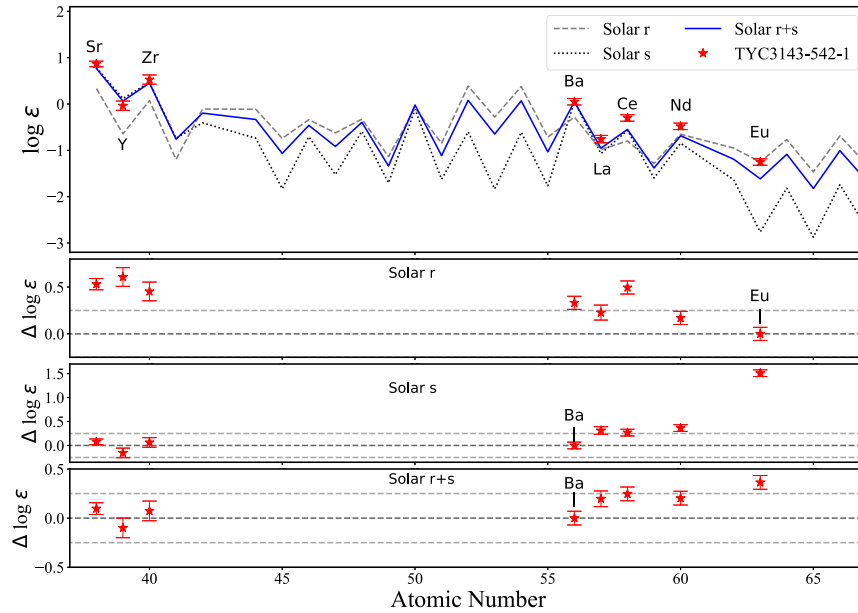


Figure 5. Similar to Figure 3, but for TYC 3143-542-1.

## Acknowledgments

Our research is supported by the National Key R&D Program of China No. 2019YFA0405502, the National Natural Science Foundation of China under grant Nos. 12090040, 12090044, 11833006, 12022304, 11973052, 11973042 and U2031144. We acknowledge the science research grants from the China Manned Space Project with NO.CMS-CSST-2021-B05. We acknowledge the anonymous referee for the suggestions that helped to largely improve the paper. H.-L.Y. acknowledges the supports from Youth Innovation Promotion Association (id. 2019060), Chinese Academy of Sciences. Physics Frontier Center/JINA Center for the Evolution of the Element (JINA-CEE), awarded by the US National Science Foundation. This work is also partially supported by the Open Project Program of the Key Laboratory of Optical Astronomy, National Astronomical Observatories, Chinese Academy of Sciences. Guo Shou Jing Telescope (the Large Sky Area Multi-Object Fiber Spectroscopic Telescope, LAMOST) is a National Major Scientific Project built by the Chinese Academy of Sciences. Funding for the project has been provided by the National Development and Reform Commission. LAMOST is operated and managed by the National Astronomical Observatories, Chinese Academy of Sciences.

## ORCID iDs

Xiao-Jin Xie <https://orcid.org/0000-0002-4440-4803>  
 Jian-Rong Shi <https://orcid.org/0000-0002-0349-7839>  
 Tian-Lu Chen <https://orcid.org/0000-0002-2944-2422>  
 Tian-Yi Chen <https://orcid.org/0000-0002-6448-8995>  
 Shuai Liu <https://orcid.org/0000-0001-5193-1727>

## References

- Abomalima, A., & Frebel, A. 2018, *ApJS*, **238**, 36  
 Aoki, M., Ishimaru, Y., Aoki, W., & Wanajo, S. 2017, *ApJ*, **837**, 8  
 Asplund, M., Grevesse, N., Sauval, A. J., & Scott, P. 2009, *ARA&A*, **47**, 481  
 Barklem, P. S., Christlieb, N., Beers, T. C., et al. 2005, *A&A*, **439**, 129  
 Beers, T. C., & Christlieb, N. 2005, *ARA&A*, **43**, 531  
 Brauer, K., Ji, A. P., Drout, M. R., & Frebel, A. 2021, *ApJ*, **915**, 81  
 Burbidge, E. M., Burbidge, G. R., Fowler, W. A., & Hoyle, F. 1957, *RvMP*, **29**, 547  
 Cameron, A. G. W. 1957, *PASP*, **69**, 201  
 Carlberg, J. K., Cunha, K., Smith, V. V., & Majewski, S. R. 2012, *ApJ*, **757**, 109  
 Chen, T.-Y., Shi, J.-R., Beers, T. C., et al. 2021, *RAA*, **21**, 036  
 Christlieb, N., Beers, T. C., Barklem, P. S., et al. 2004, *A&A*, **428**, 1027  
 Côté, B., Eichler, M., Arcones, A., et al. 2019, *ApJ*, **875**, 106  
 Côté, B., Fryer, C. L., Belczynski, K., et al. 2018, *ApJ*, **855**, 99  
 Cowan, J. J., Sneden, C., Lawler, J. E., et al. 2021, *RvMPh*, **93**, 015002  
 Cui, X.-Q., Zhao, Y.-H., Chu, Y.-Q., et al. 2012, *RAA*, **12**, 1197  
 Ezzeddine, R., Rasmussen, K., Frebel, A., et al. 2020, *ApJ*, **898**, 150  
 Farouqi, K., Kratz, K. L., Pfeiffer, B., et al. 2010, *ApJ*, **712**, 1359  
 Farouqi, K., Thielemann, F.-K., Rosswog, S., & Kratz, K.-L. 2021, [arXiv:2107.03486](https://arxiv.org/abs/2107.03486)  
 Fernández-Trincado, J. G., Beers, T. C., Queiroz, A. B. A., et al. 2021, *ApJL*, **918**, L37  
 Fujimoto, S.-i., Nishimura, N., & Hashimoto, M.-a 2008, *ApJ*, **680**, 1350  
 Gaia Collaboration 2018, *A&A*, **616**, A1  
 Grichener, A., & Soker, N. 2019, *ApJ*, **878**, 24  
 Guadin, D., Shank, D., Beers, T. C., et al. 2021, *ApJ*, **908**, 79  
 Gull, M., Frebel, A., Hinojosa, K., et al. 2021, *ApJ*, **912**, 52  
 Gustafsson, B., Edvardsson, B., Eriksson, K., et al. 2008, *A&A*, **486**, 951  
 Hansen, T. T., Holmbeck, E. M., Beers, T. C., et al. 2018, *ApJ*, **858**, 92  
 Holmbeck, E. M., Hansen, T. T., Beers, T. C., et al. 2020, *ApJS*, **249**, 30  
 Hotokezaka, K., Beniamini, P., & Piran, T. 2018, *IJMPD*, **27**, 1842005  
 Kasen, D., Metzger, B., Barnes, J., Quataert, E., & Ramirez-Ruiz, E. 2017, *Natur*, **551**, 80  
 Lattimer, J. M., & Schramm, D. N. 1974, *ApJL*, **192**, L145  
 Mashonkina, L., & Gehren, T. 2001, *A&A*, **376**, 232  
 Mashonkina, L., Gehren, T., & Bikmaev, I. 1999, *A&A*, **343**, 519  
 Mirizzi, A. 2015, *PhRvD*, **92**, 105202



- Naidu, R. P., Ji, A. P., Conroy, C., et al. 2022, *ApJL*, **926**, L36
- Nishimura, N., Takiwaki, T., & Thielemann, F.-K. 2015, *ApJ*, **810**, 109
- Obergaulinger, M., Just, O., & Aloy, M. A. 2018, *JPhG*, **45**, 084001
- Pancino, E., Romano, D., Tang, B., et al. 2017, *A&A*, **601**, A112
- Papish, O., Soker, N., & Bukay, I. 2015, *MNRAS*, **449**, 288
- Pfeiffer, M. J., Frank, C., Baumüller, D., Fuhrmann, K., & Gehren, T. 1998, *A&AS*, **130**, 381
- Pian, E., D'Avanzo, P., Benetti, S., et al. 2017, *Natur*, **551**, 67
- Reetz, J. 1991, Diploma thesis, PhD thesis, München University
- Roederer, I. U., Preston, G. W., Thompson, I. B., et al. 2014, *AJ*, **147**, 136
- Roederer, I. U., Sakari, C. M., Placco, V. M., et al. 2018, *ApJ*, **865**, 129
- Rosswog, S., Korobkin, O., Arcones, A., Thielemann, F. K., & Piran, T. 2014, *MNRAS*, **439**, 744
- Sakari, C. M., Placco, V. M., Farrell, E. M., et al. 2018, *ApJ*, **868**, 110
- Sato, K. 1974, *PThPh*, **51**, 726
- Siegel, D. M. 2019, *EPJA*, **55**, 203
- Siegel, D. M., Barnes, J., & Metzger, B. D. 2019, *Natur*, **569**, 241
- Sitnova, T., Zhao, G., Mashonkina, L., et al. 2015, *ApJ*, **808**, 148
- Sitnova, T. M., Mashonkina, L. I., & Ryabchikova, T. A. 2013, *AstL*, **39**, 126
- Snedden, C., Cowan, J. J., & Gallino, R. 2008, *ARA&A*, **46**, 241
- Snedden, C., Preston, G. W., McWilliam, A., & Searle, L. 1994, *ApJL*, **431**, L27
- Symbalysty, E. M. D., Schramm, D. N., & Wilson, J. R. 1985, *ApJL*, **291**, L11
- Thielemann, F. K., Eichler, M., Panov, I. V., & Wehmeyer, B. 2017, *ARNPS*, **67**, 253
- Tsujimoto, T. 2021, *ApJL*, **920**, L32
- Watson, D., Hansen, C. J., Selsing, J., et al. 2019, *Natur*, **574**, 497
- Witti, J., Janka, H. T., & Takahashi, K. 1994, *A&A*, **286**, 841
- Xing, Q.-F., Zhao, G., Aoki, W., et al. 2019, *NatAs*, **3**, 631
- Yamazaki, Y., Kajino, T., Mathews, G. J., et al. 2021, arXiv:2102.05891
- Yan, H., Li, H., Wang, S., et al. 2022, *The Innovation*, **3**, 100224
- Yan, H.-L., Shi, J.-R., Zhou, Y.-T., et al. 2018, *NatAs*, **2**, 790
- Zhao, G., Mashonkina, L., Yan, H. L., et al. 2016, *ApJ*, **833**, 225